1 Introduction

Real outbreaks have significant heterogeneity in secondary case distributions – including "superspreading," marked by a small fraction of individuals causing a disproportionately large fraction of realized transmission [6, 13]. Several distinct factors influence who becomes a superspreader and can disproportionately affect outbreak dynamics [5, 12]. Superspreading can help explain why epidemics break- and burn out in some times and places but not others, despite apparently similar contexts. Furthermore, control efforts that incorporate superspreading into their design may be more effective [1, 8, 11]. Superspreading may be most salient for disease dynamics and control strategies at the time of outbreak [2]. For this reason, theoretical treatment of superspreading emphasizes individual-level transmission patterns, often while assuming a fully susceptible population. Over longer timescales, the processes of susceptible depletion and resupply, which are elegantly captured in mechanistic compartmental models, drive population-scale disease dynamics. Despite shared theory motivating models that highlight individual-level transmission events and superspreading, and those that highlight population-level transmission dynamics, there remains a gap between how each model framework treats individual-level transmission heterogeneity.

Theoretical treatment of superspreading has focused on effective, non-mechanistic models that link observed secondary case counts to a continuous random variable, the "individual reproduction number," via a Poisson sampling process[6]. In this way, variation from the stochastic process of successful transmission is conceptually separated from a more intrinsic individual-level heterogeneity [in expected infectiousness] that may emerge from a plethora of potential differences in physiology, contact patterns, or behaviors between individuals.

In its simplest form, the canonical ODE S[E]IR model assumes homogeneous rates of recovery and constant, uniform infectivity across all individuals during the infectious stage [3, 4]. Although single-infective-class compartmental models would seem ill-equipped to describe heterogeneity, even the SIR model yields exponentially distributed recovery times and thus, when linearized, geometric secondary case distributions. Further, taking susceptible depletion into account, the exponentially-distributed durations still drive variation in the number of infections attributable to fractions of the population infected at a given time, while a changing effective reproduction number drives variation between fractions of the population infected at different times. In other words, even fully deterministic ODE models predict variation around $\mathcal{R}_0$ in the expected number of cases per case. We term this variation, "emergent heterogeneity." In practice, epidemiological modelers also include *explicit heterogeneity* into their models, for example by considering age- or spatially-explicit compartments that may have different expected rates of mixing, transmission, or recovery [10]. Explicit heterogeneity reproduces superspreading in linear compartmental models [7].

We delineate the distinct sources of individual variation in transmission inscribed into a simple SIR model. We trace how these sources compose into observed or observable heterogeneity in different settings, for example contrasting

how heterogeneity emerges in dynamical models versus linearized, or branching-process models. Throughout, we highlight the understudied but critically important role of disease dynamics *per se* in generating individual-level heterogeneity. We aim to spur the development of theory and methods that better integrate heterogeneity and dynamics, ultimately facilitating feedback between data on incidence and individual-level transmission chains, mechanistic model specification, identification, and validation, and intervention design.

2 Box: Kappa tutorial

Box 1. κ tutorial.

For a continuous distribution with mean μ and variance σ^2, the (generalized) *dispersion parameter*, κ, is defined as the squared coefficient of variation σ^2/μ^2. The dispersion parameter of a discrete distribution with mean μ and variance σ^2 is defined as $\kappa_{\mathrm{discrete}} = (\sigma^2 - \mu)/\mu^2$.

The statistics κ and $\kappa_{\mathrm{discrete}}$ have desirable properties for a dispersion measure: They *increase* with dispersion around the mean and equal zero for a Dirac delta function.

The dispersion parameter is *invariant* under Poisson mixing. When a gamma distribution is parameterized by its mean μ and dispersion κ, the resulting negative binomial distribution, derived from Poisson mixing, is likewise parameterized by μ and $\kappa_{\mathrm{discrete}} = \kappa$. The connection between κ and $\kappa_{\mathrm{discrete}}$ holds for Poisson mixture with any mixing distribution.

In our setting, the continuous distribution corresponds to the expected transmission rate, and the discrete distribution arises from the stochastic realization of that rate, i.e., by compounding a Poisson distribution with a rate parameter derived from the continuous distribution. Hence, κ and $\kappa_{\mathrm{discrete}}$ can be used to characterize the dispersion of secondary case distributions.

3 Results

Demographic stochasticity can generate "emergent" heterogeneity even in the absence of explicit differences between individual-based rates (Figure 1). In simple models, this heterogeneity can be characterized. We explicate the notion that this is predictable (see Box). [**JD:** *Is that really what Box is doing, though? Or more about linking the emergent stochasticity in the deterministic vs. demographic-stochastic models?*]

The inequality in the secondary cases, i.e., the relationship between the fraction of new infections and the fraction of infectors, varied by $\mathcal{R}_0$; the inequality in the activity distribution did not. The share of Poisson noise in the inequality shrank in epidemics with large $\mathcal{R}_0$(Figure 1, right panel).

The left panel of Figure 1 shows patterns of emergent heterogeneity in secondary case numbers during the early stage of an outbreak, when the population
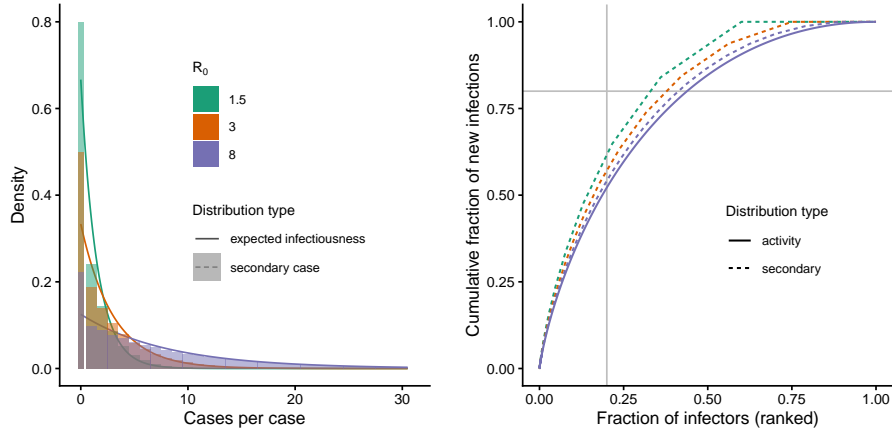
Figure 1: **Heterogeneity emerges even from a simple, linearized compartmental model** due to implicit variation in recovery times among infectors. (left) Activity distributions (density curves) and secondary case distributions (density histograms) for the outset of an SIR epidemic. Because the first bin (at zero) sits at the boundary of support for each distribution, we have plotted this bin as double the density and half the width; this adjustment preserves area-to-area correspondence with the PDF, while facilitating visual comparison of the heights of the density and mass functions. (right) Inequality curves for *activity* distributions from SIR models with differing $\mathcal{R}_0$ are identical (and indistinguishable due to overplotting); inequality in the *case* distribution decreases with $\mathcal{R}_0$ towards the theoretical limit of the activity distribution.

is fully susceptible. Both activity distribution and secondary case distribution depend on $\mathcal{R}_0$. How would the secondary distribution look if we examined all infectors over the entire outbreak? To address this, we simulated epidemic outbreaks with different $\mathcal{R}_0$ values in a population of 10000. For each infected individual, we recorded the number of secondary cases they generated during the outbreak. The top row of Figure 2 shows realized distributions of "offspring cases" caused by individual infectors in simple, stochastic SIR epidemics. Unlike in the linearized case above, the distributions remain indistinguishable across a wide range of the key parameter $\mathcal{R}_0$. This seems surprising: in particular, we see much greater dynamical changes when $\mathcal{R}_0$ is large; we might expect this to be reflected in a larger variation in the offspring distribution.

To reconcile these two observations, we examined how heterogeneity differs when analyzing epidemiologically relevant cohorts, which are groups of individuals infected at the same time, as the outbreak unfolds. A large $\mathcal{R}_0$ results in a large initial number of cases per case; however, rapid depletion of susceptible individuals reduces the chance of large secondary cases. In contrast, a small $\mathcal{R}_0$ produces fewer initial cases per case, but the slower susceptible exhaustion allows for larger secondary cases (Figure S1). We then split the total case-per-case variance over the course of the outbreak into between- and within-cohort components. We found that epidemics with larger $\mathcal{R}_0$ have larger between-cohort variation, as expected. However, this is balanced by smaller within-cohort variation (Figure 2, lower panel). We can in fact prove that the variance in case-per-case, conditioned on the entire outbreak, is equal to one, regardless of the value of $\mathcal{R}_0$ (Section S.1).

We are also interested in what emergent distributions will look like to people studying outbreaks in real time. We are interested, at least to some extent, both in how cohorts change through time, and in what the outbreak will "look like" if we observe from a particular time. To do so, we simulated a deterministic SIR model and stopped it at different cutoff points. At each time point, we calculated case-per-case heterogeneity based on the cases generated up to that time by infected cohorts. We found that in the early stage of the outbreak, the observed heterogeneity was lower than that observed in the linearized model or throughout the entire outbreak, and that it varied by $\mathcal{R}_0$ (Figure 3). By the end of the outbreak, the heterogeneity in case-per-case for different values of $\mathcal{R}_0$ became indistinguishable and equal to one.

We also examined an idealized scenario in which, for each time point, we computed case-per-case heterogeneity over the entire outbreak, considering all cohorts that had become infectious up to that time. In epidemics with lower $\mathcal{R}_0$, the case-per-case mean and variance across early-infected cohorts were the same as those in a linearized model (Figure 4). Incorporating cohorts who later, but prior to the outbreak peak, became infected reduced variability. Further incorporating those cohorts that became infected after the peak increased the variability. By the end of the outbreak, all epidemics with different $\mathcal{R}_0$ agreed on the case-per-case heterogeneity, measured by κ.
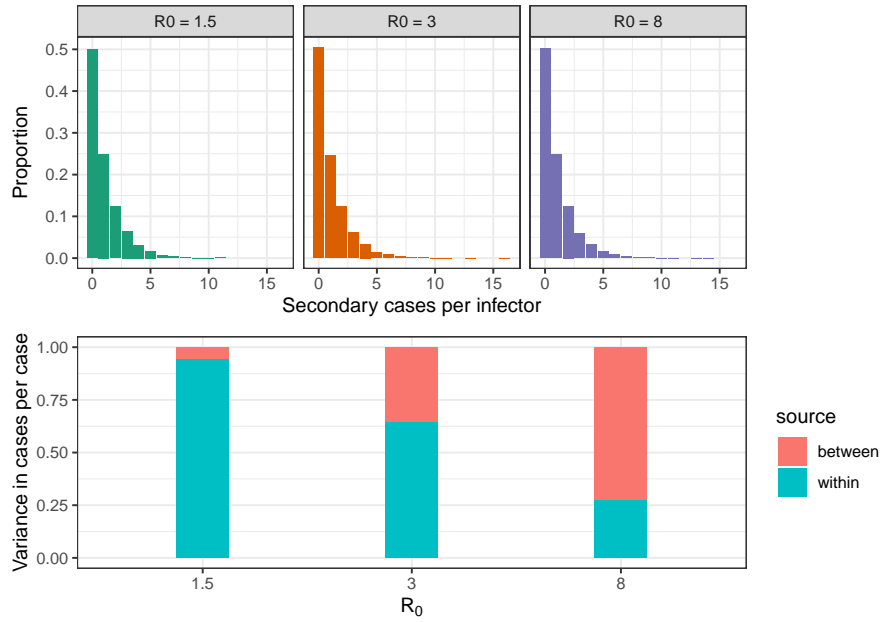
4

Figure 2: **Indistinguishable empirical distributions of case-per-case for epidemics of different strengths conditioned over the entire outbreak cycle.** Epidemic outbreaks have been simulated for a population of 10000 with different $\mathcal{R}_0$ and the number of secondary cases per infector has been recorded at the time of outbreak extinction (top panels). Identical variance in case-per-case for epidemics of different strengths modeled using simple compartmental models (lower panel). As $\mathcal{R}_0$ increases, between-cohort variance rises, and within-cohort variance falls, maintaining constant total variance of one.
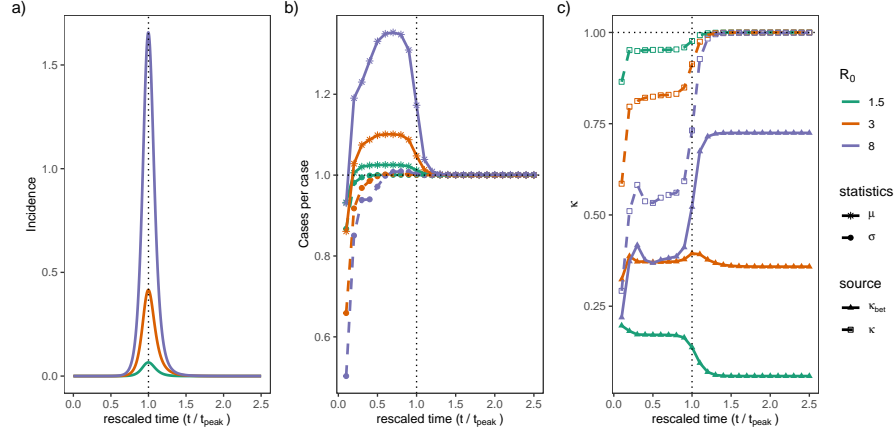
Figure 3: **Distribution of case-per-case evolves over the course of outbreak.** Panel a: The size of the cohort infected at each rescaled time point is measured by incidence at that point. Panel b: The mean and standard deviation of case-per-case at each time are computed using the realized cases up to that point. After the peak, the standard deviation has already settled at one; the mean approaches one rapidly, regardless of $\mathcal{R}_0$. Panel c: The squared coefficient of variation of case-per-case κ climbs over the course of the outbreak. Epidemics with small $\mathcal{R}_0$ take longer to reach their peak. Even early on, differences in how long people remain infectious in the same cohort become important, making the within component of κ larger (and, as a result, decreasing the between component part). In epidemics with large $\mathcal{R}_0$, as opposed to those with $\mathcal{R}_0$ close to one, the between-cohort component jumps after the outbreak peak as the susceptible pool depletes. For panels b and c, the simulation was stopped at each time point to compute the y-axis value. The y-axis value at each time point was computed by assigning to each cohort the number of realized cases up to that time. In all panels, time units measured in the mean infectious period are again scaled relative to the peak time.

4 Discussion

In SIR-type epidemics, the effective reproduction number declines as the susceptible population becomes depleted. Consequently, if surveillance begins after the initial transmission generations, estimates of cases-per-case will represent the reduced effective reproduction number rather than $\mathcal{R}_0$[9]. As a result, delayed surveillance may yield substantially lower estimates, especially when $\mathcal{R}_0$ is large, due to rapid depletion of the susceptible pool.
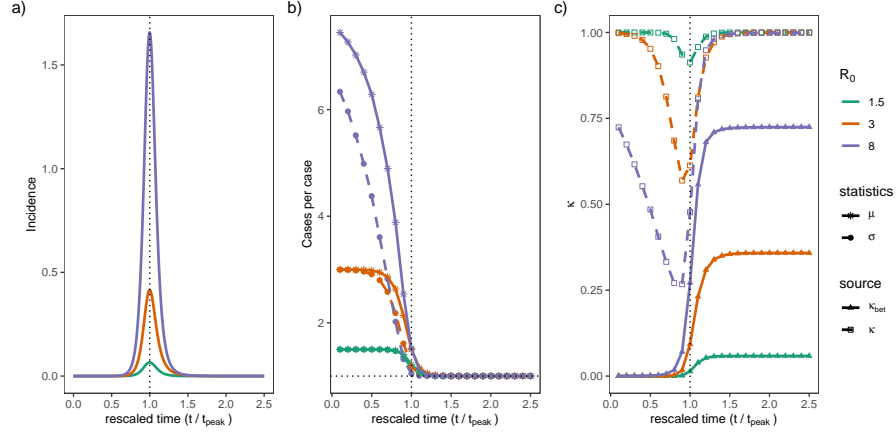
Figure 4: **Nowcasting the case-per-case distribution evolves as the outbreak unfolds.** Panel a: Incidence represents the size of each cohort infected at each rescaled time point. By "rescaled," we mean that time has first been scaled by the mean infectious period and is then measured relative to the outbreak peak. Panel b: At each time, the mean and standard deviation of cases caused by each case are calculated using only cohorts infected up to that time. The mean cases per case is larger in early-infected cohorts and depends on the key parameter $\mathcal{R}_0$. As time goes by, later-infected cohorts have larger weights, as measured by incidence. These cohorts experience susceptible pool depletion, leading to fewer secondary cases and a lower mean case-per-case number. After the peak, the susceptible population size stabilizes, and the mean and variance approach one. Panel c: The between-cohort component of the squared coefficient of variation κ_{bet} is negligible among the early-infected cohorts, as they experience a similar size of susceptibles. As the outbreak unfolds, the decline in the susceptible population drives between-cohort variation, which is more pronounced in epidemics with large $\mathcal{R}_0$. The squared coefficient of variation κ reaches its minimum around the outbreak peak; the largest cohort, measured by incidence, experiences a sharp depletion of susceptibles, and the impact of variation in recovery time fades—declining the variance and, in turn, κ. After the peak, κ rebounds to one. For panels b and c, the y-axis value at each time point was computed using only the cohorts that had been infected up to that time.

5   Materials and Methods

The values of secondary cases in the left panel of Figure 1, were generated by computing the geometric probability density function with mean $\mathcal{R}_0$ at the points $0, 1, \ldots, 30$. As for the expected infectiousness, we evaluated the exponential probability density function with mean $\mathcal{R}_0$ at 300 equally distanced point in the interval $[0, 30]$.

In the right panel of Figure 1, we used the Lloyd-Smith's approach to compute the inequality in the activity distribution. More specifically, we used the relation $F_{\text{trans}}(x) = \frac{1}{\mathcal{R}_0^2} \int_0^x v e^{-\frac{1}{\mathcal{R}_0}} dv$ which is the fraction of cases due to those caused up to x secondary cases. The fraction of cases due to those caused more than x cases would be $1 - F_{\text{trans}}(x)$, which is equal to $(1 + \frac{x}{\mathcal{R}_0}) e^{-\frac{x}{\mathcal{R}_0}}$. The population fraction of the individuals infected more than x cases is $e^{-\frac{v}{\mathcal{R}_0}}$. We used a similar approach to compute the inequality in the secondary case distribution: We used the relation $F_{\text{trans}}(x) = \frac{1}{\mathcal{R}_0} \sum_{v=0}^x v G(v, \mathcal{R}_0)$ which is the fraction of cases due to those caused up to x secondary cases. Here $G(v, \mathcal{R}_0)$ is a geometric distribution with mean $\mathcal{R}_0$. The fraction of cases due to those caused more than x cases equals $1 - F_{\text{trans}}(x)$. The population fraction of these individuals would be $1 - P(x)$, where $P(x)$ is the cumulative distribution function of a geometric distribution with mean $\mathcal{R}_0$ evaluated at x.

To generate the top panel of Figure 2, we used the individual based simulation and computed the case per case reproductive number in a population of size 10^4. The simulation was initiated with one case.

We used a deterministic SIR model to compute the mean and variance of $\mathcal{R}_c$. First, we scaled time by the mean infectious period, so the resulting SIR model then depends on one parameter: $\mathcal{R}_0$. The SIR differential equations were numerically solved for the proportions of susceptible $x(t)$ and infectious $y(t)$ at each time point t. The time interval for integration was set to $[0, 100]$, well after the outbreak died out. We then used the **R** function `approxfun` to construct a function, $X(t)$, that linearly interpolates the time-series $(t, \mathcal{R}_0 x(t))$. We associated a cohort to each of the first 60% time points in the time-series t (We used a 60% cutoff to ensure cohorts had almost recovered by the end of the simulation period) and calculated the cohort-specific mean and variance. More specifically, for the cohort infected at time point τ, the mean, $\mu(\tau)$, and variance $\sigma^2(\tau)$ of $\mathcal{R}_c$ read as:

$$\mu(\tau) = \int_{t > \tau} f(t - \tau) \int_\tau^t \mathcal{R}_0 x(s) ds \, dt \,,$$

$$\mathbb{E}[\mathcal{R}_c^2(\tau)] = \int_{t > \tau} f(t - \tau) \left(\int_\tau^t \mathcal{R}_0 x(s) ds \right)^2 dt \,,$$

$$\sigma^2(\tau) = \mathbb{E}[\mathcal{R}_c^2(\tau)] - \mu^2(\tau).$$

To calculate these quantities for the cohort infected at τ, the interpolating function $X(t)$ was integrated from τ to t, which is the case reproductive potential associated with the cohort fraction recovered at time point t. The mean $\mathcal{R}_c$ for each cohort $\mu(\tau)$ was then the integral of the case reproductive potential weighted by the infectious period density function. We used the same approach to compute $E[\mathcal{R}_c^2(\tau)]$ and the variance of $\mathcal{R}_c$ for each cohort $\sigma^2(\tau)$. In Figure S1, the middle panel was generated using this approach.

We obtained the mean of $\mathcal{R}_c$ by integrating the cohort-specific mean $\mu(\tau)$ against the incidence, $i(t) = \mathcal{R}_0 x(t) y(t)$, and normalizing the result by the final size, $\int i(t) dt$. We computed the between variance by integrating over the

cohort's mean $\mu(\tau)$ weighted by the incidence. The result was then normalized by the final size. The with-in cohort variance was computed by taking integral over the cohorts' variance $\sigma^2(\tau)$ weighted by the incidence. The result was also normalized by the final size. The total variance was the sum of the between and with-in variances. We also calculated the total variance independently; we integrated $\mathbb{E}[\mathcal{R}_c^2(\tau)]$ weighted by the incidence and divided it by the final size. The result minus the squared mean of $\mathcal{R}_c$ yielded the total variance. Both approaches produced the same value for the total variance.

All integrations were done using `lsoda` method with the **R** package `deSolve`. All simulations were carried out using **R 4.5.2**. Code for all numerical simulations is housed at: `https://github.com/dushoff/kappaCode`.

We solved all integrals across a range of values for $\mathcal{R}_0$, using the starting values $y_0 = 10^{-9}; x_0 = 1 - 10^{-9}$ to represent the limiting case in which there are no exogenous cases. In building these simulations, we used a range of time step sizes, noting convergence towards known and conjectured values (e.g., epidemic final size, mean case reproduction number, variance in case reproduction number) as resolution increased.

S.1   Analytical Results

S.1.1   Preliminaries

The standard SIR model is described by the following equations:

$$\dot{x} = -\mathcal{R}_0 xy,$$
$$\dot{y} = \mathcal{R}_0 xy - y,$$

where $x(t)$ and $y(t)$ denote the proportion of susceptible and infectious individuals, respectively. Time has been normalized by the recovery rate. Let $i(t)$ denote the incidence $\mathcal{R}_0 xy$, and define the size of the epidemic as follows:

$$Z = \int_0^\infty dt\, i(t).$$

Let f denote the distribution of residence times in the infectious compartment. Define $F(t)$ as the corresponding survival distribution, that is

$$F(t) = 1 - \int_0^t d\tau f(\tau) = \int_t^\infty d\tau f(\tau). \tag{S.1}$$

Note that $F(t)$ is the probability that an individual infected at time 0 remains infectious after time t.

We define the *expected case reproductive number* between time τ and ρ as

$$C(\tau, \rho) = \mathcal{R}_0 \int_\tau^\rho dt\, x(t).$$

The kth weighted raw moment of C is then defined as

$$C_k = \int_0^\infty d\tau \int_\tau^\infty d\rho \; w(\tau, \rho)(C(\tau, \rho))^k, \qquad \text{(S.2)}$$

where $w(\tau, \rho) = i(\tau)f(\rho - \tau)$ is the size of the cohort that became infectious at time τ and recovered at time ρ.

S.1.2 The Statement

The excess variation of the individual case reproductive number in the standard SIR model outbreak is 1. Mathematically, this amounts to proving that

$$\boxed{\kappa_C = \frac{C_0 C_2}{C_1^2} - 1 = 1.} \qquad \text{(S.3)}$$

S.1.3 Proof

We will calculate C_0, C_1 and C_2. We can calculate C_0 and C_1 without making any assumptions about the functional form of f (we don't have to assume that the wait times are exponentially distributed). We do need F to be memoryless, i.e., obey $F(a + b) = F(a)F(b)$, to get the "right" value of C_2. Calculating each of these moments essentially involves multiple manipulations of the limits of the integrals involved.

From Equation S.2, we have

$$C_0 = \int_0^\infty d\tau \int_\tau^\infty d\rho \; w(\tau, \rho)$$
$$= \int_0^\infty d\tau \int_\tau^\infty d\rho \; i(\tau)f(\rho - \tau)$$

Substituting $\omega + \tau$ for ρ in the inner integral, results in

$$C_0 = \int_0^\infty d\tau \; i(\tau) \int_0^\infty d\omega \; f(\omega).$$

Since f is the residence time distribution (note we're not invoking the fact that f is an exponential distribution!), the inner integral is simply 1. It follows that

$$C_0 = \int_0^\infty d\tau \; i(\tau)$$
$$= Z.$$

The next step is to prove that $C_1 = Z$. From Equation S.2, we have

$$C_1 = \int_0^\infty d\tau \int_\tau^\infty d\rho \; w(\tau, \rho)C(\tau, \rho)$$
$$= \mathcal{R}_0 \int_0^\infty d\tau \int_\tau^\infty d\rho i(\tau)f(\rho - \tau) \int_\tau^\rho dt x(t).$$

Instead of first integrating over t from τ to ρ and then over ρ from τ to ∞, we can first integrate over ρ from t to ∞ and then integrate over t from τ to ∞, i.e.,

$$C_1 = \mathcal{R}_0 \int_0^\infty d\tau \int_\tau^\infty dt\, i(\tau)x(t) \int_t^\infty d\rho f(\rho - \tau).$$

Substitute $\rho = \omega + \tau$ in the innermost integral and using Equation S.1, we get

$$C_1 = \mathcal{R}_0 \int_0^\infty d\tau \int_\tau^\infty dt\, i(\tau)x(t) \int_{t-\tau}^\infty d\omega f(\omega)$$

$$= \mathcal{R}_0 \int_0^\infty d\tau \int_\tau^\infty dt\, i(\tau)x(t)F(t - \tau).$$

Note again that we have not used the fact that f is exponential, we have merely used the definition of F as an integral of f. By interchanging the order of the integrals once more, we have

$$C_1 = \mathcal{R}_0 \int_0^\infty d\tau \int_\tau^\infty dt\, i(\tau)x(t) \int_{t-\tau}^\infty d\omega f(\omega)$$

$$= \mathcal{R}_0 \int_0^\infty dt\, x(t) \int_0^t d\tau\, i(\tau)F(t - \tau).$$

Note that the inner integrand counts the number of individuals that entered the infectious state at some time $\tau < t$ and remain infectious at time t. When we integrate over all times $\tau < t$, we simply get the number of individuals who are infections at time t, i.e., $y(t)$. So,

$$C_1 = \mathcal{R}_0 \int_0^\infty dt\, x(t) \int_0^t d\tau\, i(\tau)F(t - \tau) \tag{S.4}$$

$$= \mathcal{R}_0 \int_0^\infty dt\, x(t)y(t) \tag{S.5}$$

$$= \int_0^\infty dt\, i(t) \tag{S.6}$$

$$= Z. \tag{S.7}$$

The next step is to show $C_2 = 2Z$. Given Equation S.2, we have

$$C_2 = \int_0^\infty d\tau \int_\tau^\infty d\rho\, w(\tau, \rho) \left(C(\tau, \rho) \right)^2$$

$$= \mathcal{R}_0^2 \int_0^\infty d\tau \int_\tau^\infty d\rho\, i(\tau)f(\rho - \tau) \left(\int_\tau^\rho dt x(t) \right)^2$$

S3

Now we break down the square integral into a double integral

$$\left(\int_{\tau}^{\rho} x(t)dt \right)^2 = \left(\int_{\tau}^{\rho} x(t)dt \right) \left(\int_{\tau}^{\rho} x(s)ds \right)$$

$$= \left(\int_{\tau}^{\rho} x(t)dt \right) \left(\int_{\tau}^{\rho} x(s)ds \right)$$

$$= \int_{\tau}^{\rho} \int_{\tau}^{\rho} dtds\, x(t)x(s).$$

In $t - s$ space, this is integrating $x(t)x(s)$ over a square region whose vertices are (τ, τ), (τ, ρ), (ρ, τ) and (ρ, ρ). This is twice the integral over the triangle whose vertices are (τ, τ), (τ, ρ) and (ρ, τ). So,

$$\left(\int_{\tau}^{\rho} x(t)dt \right)^2 = 2 \int_{\tau}^{\rho} ds \int_{\tau}^{s} dt\, x(t)x(s)$$

Plugging this back into the expression for C_2 yields

$$C_2 = 2\mathcal{R}_0^2 \int_0^{\infty} d\tau \int_{\tau}^{\infty} d\rho \int_{\tau}^{\rho} ds \int_{\tau}^{s} dt\, i(\tau)f(\rho - \tau)x(t)x(s).$$

First, we reorder the integrals over ρ and s and change the limits appropriately

$$C_2 = 2\mathcal{R}_0^2 \int_0^{\infty} d\tau\, i(\tau) \int_{\tau}^{\infty} ds\, x(s) \int_s^{\infty} d\rho \int_{\tau}^{s} dt f(\rho - \tau)x(t).$$

Next, we reorder the integrals over ρ and t to get

$$C_2 = 2\mathcal{R}_0^2 \int_0^{\infty} d\tau\, i(\tau) \int_{\tau}^{\infty} ds\, x(s) \int_{\tau}^{s} dt\, x(t) \int_s^{\infty} d\rho f(\rho - \tau).$$

By substituting $\rho = \omega + \tau$ and using Equation S.1, we get

$$C_2 = 2\mathcal{R}_0^2 \int_0^{\infty} d\tau\, i(\tau) \int_{\tau}^{\infty} ds\, x(s) \int_{\tau}^{s} dt\, x(t)F(s - \tau).$$

We then reorder the integrals over τ and s

$$C_2 = 2\mathcal{R}_0^2 \int_0^{\infty} ds\, x(s) \int_0^s d\tau \int_{\tau}^{s} dt\, x(t)i(\tau)F(s - \tau).$$

Swapping the integrals over τ and t, results in

$$C_2 = 2\mathcal{R}_0^2 \int_0^{\infty} ds\, x(s) \int_0^s dt\, x(t) \int_0^t d\tau\, i(\tau)F(s - \tau).$$

Now, we use the fact that the survival function F is memoryless, i.e., $F(a+b) = F(a)F(b)$, and replace $F(s - \tau)$ with $F(s - t)F(t - \tau)$

$$C_2 = 2\mathcal{R}_0^2 \int_0^{\infty} ds\, x(s) \int_0^s dt\, x(t) \int_0^t d\tau\, i(\tau)F(s - t)F(t - \tau).$$

S4

Next, we use the same argument we used to go from Equation S.4 to Equation S.5, which results in

$$
\begin{aligned}
C_2 &= 2\mathcal{R}_0^2 \int_0^\infty ds\, x(s) \int_0^s dt\, x(t)F(s-t)y(t) \\
&= 2\mathcal{R}_0 \int_0^\infty ds\, x(s) \int_0^s dt\, i(t)F(s-t) \\
&= 2\mathcal{R}_0 \int_0^\infty ds\, x(s)y(s) \\
&= 2 \int_0^\infty ds\, i(s) \\
&= 2Z.
\end{aligned}
$$

Finally, replacing C_0, C_1, and C_2 by Z, Z, and $2Z$, respectively, in Equation S.3, results $\kappa_C = 1$.
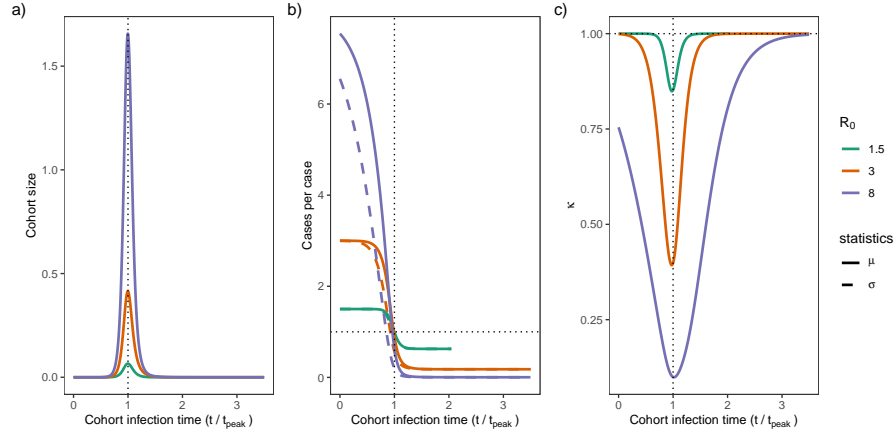
Supplementary Figures

Figure S1: **Between-cohort variation in case-per-case increases as $\mathcal{R}_0$ increases.** Panel a depicts cohort size as a function of the time of infection, in units of the mean infectious period divided by the incidence peak time; the cohort size equals the incidence. In Panel b, the mean and standard deviation of case-per-case associated with each cohort are plotted. Early in the outbreak, the susceptible pool shrinks slowly, and differences in recovery time mainly cause variations in case numbers. As a result, the average for cases is about the same as in a simple linearized model. Near the outbreak's peak, faster susceptible loss partly compensates for the inequality stemming from the infectious period, and, in turn, the squared coefficient of variation κ decreases (Panel c). After the peak, once the susceptible pool has become nearly constant again, variation in the infectious period once more drives variation within cohorts; κ approaches one. In stronger outbreaks (higher $\mathcal{R}_0$), it takes longer (in rescaled time units) for the susceptible population to stabilize, explaining the slower move of κ toward one.

References

[1] T Garske and C J Rhodes. The effect of superspreading on epidemic outbreak size distributions. *J Theor Biol*, 253:228–37, 2008.

[2] Ashish Goyal, Daniel B Reeves, and Joshua T Schiffer. Multi-scale modelling reveals that early super-spreader events are a likely contributor to novel variant predominance. *J R Soc Interface*, 19:20210811, 2022.

[3] Herbert W Hethcote. The mathematics of infectious diseases. *SIAM Review*, 42(4):599–653, 2000.

[4] W. O. Kermack and A. G. McKendrick. A contribution to the mathematical theory of epidemics. *Proceedings of the Royal Society A.*, 115(772):700–721, 1927.

[5] Elise J Kuylen, Andrea Torneri, Lander Willem, Pieter J K Libin, Steven Abrams, Pietro Coletti, Nicolas Franco, Frederik Verelst, Philippe Beutels, Jori Liesenborgs, and Niel Hens. Different forms of superspreading lead to different outcomes: Heterogeneity in infectiousness and contact behavior relevant for the case of SARS-CoV-2. *PLoS Comput Biol*, 18:e1009980, 2022.

[6] J O Lloyd-Smith, S J Schreiber, P E Kopp, and W M Getz. Superspreading and the effect of individual variation on disease emergence. *Nature*, 438:355–9, 2005.

[7] Michael T Meehan, Angus Hughes, Romain R Ragonnet, Adeshina I Adekunle, James M Trauer, Pavithra Jayasundara, Emma S McBryde, and Alec S Henderson. Replicating superspreader dynamics with compartmental models. *Sci Rep*, 13:15319, 2023.

[8] Bjarke Frost Nielsen, Kim Sneppen, and Lone Simonsen. The counterintuitive implications of superspreading diseases. *Nat Commun*, 14:6954, 2023.

[9] Lorenzo Pellis, Paul J. Birrell, Joshua Blake, Christopher E. Overton, Francesca Scarabel, Helena B. Stage, Ellen Brooks-Pollock, Leon Danon, Ian Hall, Thomas A. House, Matt J. Keeling, Jonathan M. Read, JUNIPER Consortium, and Daniela De Angelis. Estimation of reproduction numbers in real time: Conceptual and statistical challenges. *Journal of the Royal Statistical Society Series A: Statistics in Society*, 185:S112–S130, 11 2022.

[10] D Schenzle. An age-structured model of pre- and post-vaccination measles transmission. *IMA J Math Appl Med Biol*, 1:169–91, 1984.

[11] Kim Sneppen, Bjarke Frost Nielsen, Robert J Taylor, and Lone Simonsen. Overdispersion in COVID-19 increases the effectiveness of limiting nonrepetitive contacts for transmission control. *Proc Natl Acad Sci U S A*, 118, 2021.

[12] Brendan Wallace, Dobromir Dimitrov, Laurent Hebert-Dufresne, and Andrew M Berdahl. Hotspot model shows how location-based superspreading accelerates and reshapes epidemics. *PNAS Nexus*, 4:pgaf299, 2025.

[13] M E Woolhouse, C Dye, J F Etard, T Smith, J D Charlwood, G P Garnett, P Hagan, J L Hii, P D Ndhlovu, R J Quinnell, C H Watts, S K Chandiwana, and R M Anderson. Heterogeneities in the transmission of infectious agents: implications for the design of control programs. *Proc Natl Acad Sci U S A*, 94:338–42, 1997.